Carbon 123 (2017) 635–644

Contents lists available at ScienceDirect

Carbon

journal homepage: www.elsevier.com/locate/carbon

Molecular dynamics study of phonon transport in graphyne nanotubes

A. Ramazani [a, d, *], A. Reihani [b], A. Soleimani [c], R. Larson [b, d], V. Sundararaghavan [a]

[a] Department of Aerospace Engineering, University of Michigan, 1320 Beal Ave., Ann Arbor, USA
[b] Department of Mechanical Engineering, University of Michigan-Ann Arbor, 2350 Hayward St., Ann Arbor, USA
[c] Department of Physics, Amirkabir University of Technology, P.O. Box 15875-4413, Tehran, Iran
[d] Department of Chemical Engineering, University of Michigan-Ann Arbor, 2300 Hayward St., Ann Arbor, USA

ARTICLE INFO

Article history:
Received 13 June 2017
Received in revised form
25 July 2017
Accepted 31 July 2017
Available online 9 August 2017

Keywords:
Carbon nanotube
Graphyne nanotube
Molecular dynamics
Phonon density of state
Phonon dispersion relation
Thermal conductivity
Phonovoltaic

ABSTRACT

We determine the thermal conductivities of α, β, and γ graphyne nanotubes (GNTs) as well as of carbon nanotubes (CNTs) using molecular dynamics simulations and the Green-Kubo relationship over the temperature range 50–400 K. We find that GNTs demonstrate considerably lower thermal conductivity than CNTs with the same diameter and length. Among α, β, and γ-GNTs, γ-GNT has the highest thermal conductivity at all temperatures. By comparing the phonon transport properties of GNTs with CNTs, we find that as the fraction of acetylene bonds in the atomic network increases, the population of high-energy optical phonons increases. This enhances phonon-phonon scattering, and reduces the mean free path, adversely affecting the thermal conductivity of GNTs relative to CNTs. Also reducing the thermal conductivity of GNTs relative to CNTs is the considerably lower acoustic phonon group velocities for the former as well as the lower volumetric heat capacity of GNTs. Optical phonons in α-GNT are high in energy (0.26 eV) with a high population number, making them more energetic than the electronic direct band gap and significantly more energetic than the thermal energy at room temperature. Therefore, we suggest α-GNT as a potential candidate for phonovoltaic energy conversion applications.
© 2017 Elsevier Ltd. All rights reserved.

1. Introduction

Recently, there has been increasing interest in studying the thermal properties of materials, driven by both industrial demand and the desire for better fundamental understanding of conductivity mechanisms. In particular, heat dissipation in nanoscale electronic devices has necessitated a search for new heat conducting materials for future progress in electronics [1–3]. Another major body of research is the search for high figure-of-merit thermoelectric materials [4,5], and materials for novel energy conversion techniques, such as thermophotovoltaic [6,7], thermal bandgap [8], and phonovoltaic [9], which further motivates the study of thermal and electronic transport.

Carbon-based materials, with their multitude of allotropes, offer unique thermal and electronic properties which are of interest in electronics and thermoelectric applications [10,11]. Among these allotropes, graphene in the form of both two-dimensional sheets and carbon nanotubes has demonstrated an extremely large intrinsic thermal conductivity. Numerous empirical studies have been carried out to evaluate the temperature-dependent thermal conductivity of carbon nanotubes, which depends strongly on nanotube length, diameter and chirality [12]. Some experimental studies have reported thermal conductivities of 3000–3500 W m^{-1} K^{-1} for individual single (SWNT) and multiwall carbon nanotubes (MWNTs) [13–15], which exceeds that of diamond at room temperature. Li. et al. have reported an experimental value of 2400 W m^{-1} K^{-1} for a SWNT with 1.8 nm diameter and 20.5 μm length [16]. Ref [12] lists experimental measurements of thermal conductivities for SWNTs at room temperature ranging from 300 to 13350 W m^{-1} K^{-1} depending on nanotube length, diameter and measurement method.

In addition to experimental studies, molecular dynamics simulations are nowadays used to determine the thermal transport properties of carbon-based materials. Classical MD simulations do not include the electronic contributions to thermal conductivity. However, since the phonon contribution to the thermal conductivity of carbon nanotubes is dominant at all temperatures [17–20], neglecting the electronic effect can be justified. In addition, MD

* Corresponding author. Department of Aerospace Engineering, University of Michigan, 1320 Beal Ave., Ann Arbor, USA.
E-mail address: ramazani@umich.edu (A. Ramazani).

http://dx.doi.org/10.1016/j.carbon.2017.07.093
0008-6223/© 2017 Elsevier Ltd. All rights reserved.

simulations provide atomistic information, which can be used for detailed analysis of spectral dependence of phonon transport in materials [21], and to determine the dominant modes of heat transfer at each condition. Numerous such studies using different classical MD techniques including those based on the Green-Kubo relationship [18,22,23], as well as non-equilibrium MD (NEMD) [24–26], reverse NEMD (RNEMD) [27–29], and homogenous NEMD (HNEMD) [30,31] simulations have been carried out to determine the thermal conductivity of carbon nanotubes and other carbon based materials.

Overall, the temperature dependence of thermal conductivity in CNTs is divided into two regimes with a peak in thermal conductivity occurring at around 300 K [22,32]. In the high temperature regime, the thermal conductivity decreases with increasing temperature due to Umklapp scattering. In the low temperature regime, Umklapp scattering is suppressed and inelastic phonon scattering occurs mostly due to fixed system boundaries. Therefore, the phonon relaxation time remains constant, and thermal conductivity demonstrates the same temperature dependence as heat capacity, which is a monotonic increase with temperature.

First suggested by Ref. [33], graphyne is a class of graphene allotropes which contains carbon triple bonds. Its atomic structure has three main symmetric types; α, β, γ graphyne (structures are shown in Fig. 1) with 33.3%, 28.6%, and 20.0% carbon triple bonds respectively. Similar to CNTs, graphyne nanotubes can be formed by rolling up the graphyne sheet into cylinders. The thermal transport properties of graphyne nanotubes (GNTs) have been far less investigated to date. A number of MD calculations have determined the thermal conductivity of graphyne sheets and nanostructures. For example, Zhang et al. [28] have performed NEMD simulations to determine the thermal conductivity of graphene and γ-graphyne sheets in the temperature range of 200–800 K. They showed that as the temperature increases the thermal conductivity decreases monotonically. They reported that the acetylenic bonds in γ-graphyne cause a significant reduction in thermal conductivity in comparison to graphene sheets, mainly due to the low atom density and weak C–C bonds in the graphyne structure. In addition, a strong directional anisotropy in the thermal conductivity of graphyne sheets was reported. Pan et al. [34] carried out NEMD simulations of γ-graphyne nanoribbons at various temperatures and reported a strong orientation dependence in thermal conductivity. They also found a higher value of thermal conductivity for armchair γ-graphyne nanoribbon than for the zigzag forms. This was attributed to more phonon transport channels and higher phonon group velocity in armchair γ-graphyne nanoribbon over the whole frequency range, relative to the other forms. It was also shown as the temperature rises from 200 K to 800 K, the thermal conductivity decreases [34]. Hu et al. [35] performed NEMD simulations on a perfect γ-graphyne nanotube (γ-GNT), and reported an extremely low thermal conductivity (below 10 W/m K at room temperature), which they attributed to the atomic structure of γ graphyne, which consists of weak acetylenic bonds and strong hexagonal (sp^2 C–C) bonds, which have a large vibrational mismatch. They indicated that, because of the large number of

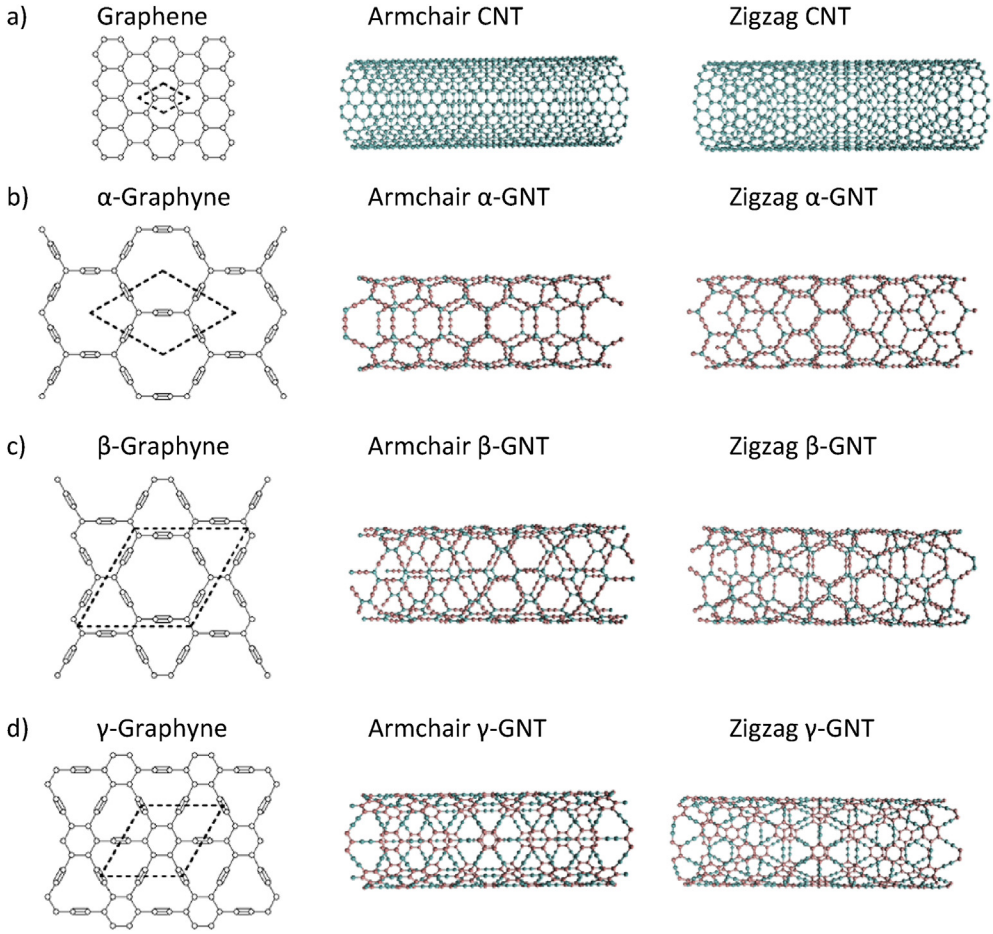

Fig. 1. Schematic representation of: (a) graphene sheet, armchair CNT, and zigzag CNT, (b) α-graphyne sheet, armchair α-GNT, zigzag α-GNT, (c) β-graphyne sheet, armchair β-GNT, zigzag β-GNT, (d) γ-graphyne sheet, armchair γ-GNT, zigzag γ-GNT. Unit cells are enclosed in dashed lines. (A colour version of this figure can be viewed online.)

acetylenic bonds, the thermal transport in GNTs is dominated by low frequency longitudinal modes [35].

In the current study, we employ MD simulations utilizing Green-Kubo method to explore thermal transport properties of α, β, and γ-GNTs in both zigzag (n, 0) and armchair (n, n) forms in the temperature range of 50 K–400 K. Phonon dispersion relations of each type of nanotubes are calculated and used to determine phonon transport parameters such as spectral phonon relaxation times, mean free path, and group velocity. Comparing these parameters to those of CNTs, the role of acetylenic bond on the phonon transport properties of carbon nanotubes is determined. This is the first study that calculates the effect of nanotube's chirality and temperature on the thermal conductivity of different phases of GNTs. It is also the first to derive phonon dispersion curves for GNTs and describe the trends in thermal conductivity based on underlying phonon transport mechanism. In addition, based on the phonon and electronic band structures, the potential application of GNTs for phonovoltaic energy conversion is suggested [9].

2. Computational method

CNT and GNT structures, depicted in Fig. 1, are modeled with a length of 50 nm and a diameter of ~1.56 nm. This diameter is appropriate for index numbers of (11, 11), (19, 0) for arm and zigzag CNTs, respectively; similarly for index numbers of (4, 4), (7, 0), for α-GNT; (4, 4), (7, 0), for β-GNTs; and (3, 3), (5, 0) γ-GNT. In Table 1, the lattice constants, carbon bond lengths, and the exact dimensions of the modeled nanotubes are reported. There are two types of C–C bonds in α and β graphyne, which have different lengths. The lengths of first type of the C–C bonds, which is present in all the modeled GNTs and CNTs, are within a narrow range of 1.405±0.015nm.

The thermal conductivity of CNTs and GNTs is determined from molecular dynamics simulations using the heat flux auto-correlation function. By means of the Green-Kubo equation within linear response theory, the thermal conductivity can be calculated as [22,36,37]:

$$\overline{\overline{K}} = \frac{V}{3k_B T_{MD}^2} \int_0^\infty \langle J(0) \cdot J(t) \rangle dt \tag{1}$$

where $\overline{\overline{K}}$ is the thermal conductivity tensor, V is the system volume, k_B is the Boltzmann constant, and T_{MD} molecular dynamics temperature. The heat flux auto-correlation function is contained within the brackets. The heat flux vector J used in Eq. (1) is defined as:

$$J = \frac{1}{V}\left[\sum_i e_i v_i - \sum_i S_i \cdot v_i\right] \tag{2}$$

Table 1
Nanotube geometry and structure dimensions of modeled nanotubes. L and D are nanotube length and diameter, α is the lattice constant. d_{s1}, d_{s2}, and d_t are lengths of first type of C–C bond, second type of C–C bond and triple bond, respectively.

Structure	L (nm)	D (Å)	α (Å)	d_{s1} (Å)	d_{s2} (Å)	d_t (Å)
GNT α-arm	50	15.40	6.98	1.40	–	1.23
GNT α-zig	50	15.56	6.98	1.40	–	1.23
GNT β-arm	50	15.72	9.50	1.39	1.46	1.23
GNT β-zig	50	15.13	9.50	1.39	1.46	1.23
GNT γ-arm	50	15.19	6.88	1.41	1.42	1.22
GNT γ-zig	50	15.34	6.88	1.41	1.42	1.22
CNT arm	50	14.92	2.46	1.42	–	–
CNT zig	50	14.88	2.46	1.42	–	–

where v_i is the velocity vector. The energy of atom i (e_i) is given as the sum of potential energy and kinetic energy (Eq. (3)) and S_i in the second term is the symmetric per atom stress tensor, which has nine components for each atom. In its general form, this stress tensor includes terms for the kinetic energy contribution, pairwise energy contribution caused by the interaction of atom i and neighbor atoms, and long range Coulombic interactions. For a more detailed description of the stress tensor, refer to ref. [38]. It is important to notice that the kinetic term of the stress tensor is excluded for all the simulations.

$$e_i = \frac{1}{2} m_i \|v_i\|^2 + U_i \tag{3}$$

The potential energy of atom i (U_i) depends upon the form of the interaction potential (including bonded and non–bonded interactions) employed in the simulations [39]. In all the simulations the second-generation reactive empirical bond order (REBO) potential is used to model the bonded carbon-carbon interactions. A cutoff distance of 0.6 nm is used for van der Waals and electrostatic interactions. Time integrations of the equations of motion are carried out using the velocity-Verlet integrator. Periodic boundary conditions are applied in all directions of the computational domain. At each simulation temperature, the system is first equilibrated for 1 ns at constant volume and temperature using the Nosé–Hoover thermostat to control the temperature. The equilibration step is followed by a 20 ns run in the microcanonical ensemble to collect data to calculate the thermal conductivity. A time step of 1 fs is used, for both equilibration and data collection runs. All simulations are performed with LAMMPS package [40].

3. Results and discussion

3.1. Thermal conductivity

The thermal conductivity tensor, $\overline{\overline{K}}$, is obtained at each MD temperature for CNTs and GNTS. Longitudinal thermal conductivities (K_{zz}) values are shown in Fig. 2(a). As can be seen, except for the β-GNT-armchair, which shows a clear peak at 75 K, the thermal conductivity values decrease with increasing MD temperature. The longitudinal thermal conductivity is significantly lower for GNTs than for CNTs. Among GNTs, the γ-GNT shows the highest thermal conductivity at all temperatures. The thermal conductivities of α-GNT and β-GNT are close to each other over the whole temperature range. No significant differences in thermal conductivity are observed between CNT and γ-GNT armchair and their corresponding zigzag nanotubes over the whole temperature range. At $T_{MD} < 200$ K, in the case of α-GNT, the armchair type shows higher thermal conductivity, while in case of β-GNT, the zigzag type shows higher thermal conductivity.

As will be discussed in Section 3.4, the Debye temperature for all the nanotubes are within or higher than the MD temperature range (50–400 °C) here, which necessitates correction of the MD calculations in order to include the quantum effects. Fig. 2(b) depicts the quantum-corrected thermal conductivity, which shows peak values at 75 °C, 75 °C, 100 °C, and 350 °C for α, β, γ-GNTs, and CNTs respectively.

Using Eq. (4), which gives the phonon contribution to thermal conductivity, the trends in thermal conductivity can be explained based on phonon heat capacity, C_{ph}, group velocity, u, and relaxation time, τ, or equivalently heat capacity, group velocity, and mean free path λ, which is integrated over the entire range of phonon frequency ν. The parameters in Eq. (4) must be obtained from the phonon density of states and dispersion relations, which are discussed in following sections.

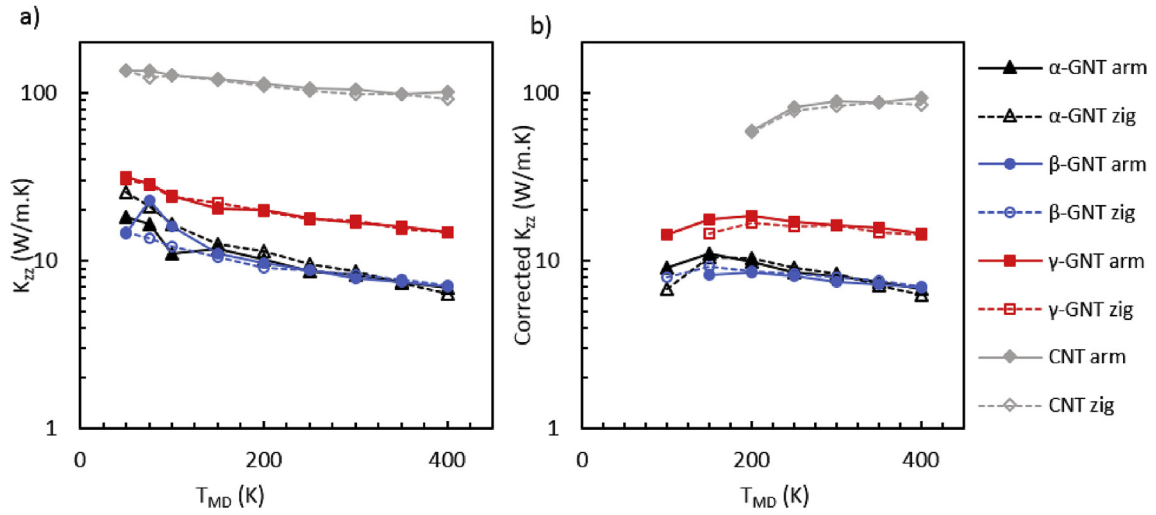

Fig. 2. Longitudinal thermal conductivity (K_{zz}) of CNTs and GNTs based on MD simulations: (a) uncorrected MD thermal conductivity (b) quantum-corrected thermal conductivity, as described in Section 3.4. (A colour version of this figure can be viewed online.)

$$K_{zz} = \int_0^{\nu_{max}} C_{ph}\, u_z^2 \tau\, d\nu = \int_0^{\nu_{max}} C_{ph}\, u_z\, \lambda\, d\nu \tag{4}$$

3.2. Phonon density of state

The total longitudinal phonon density of states (DOS) is calculated for nanotubes at each temperature by taking the Fourier transform of the velocity autocorrelation function on each atom in the system, as shown in Eq. (5).

$$D_l(\omega) = \frac{m}{k_B T_{MD}} \sum_{j=1}^{N} \int e^{-i\omega t} \langle v_{z_j}(t) v_{z_j}(0) \rangle dt \tag{5}$$

where the subscript "z" denotes the z direction, in which the nanotube is aligned, m is the atomic mass, N is the total number of atoms, ω is the phonon angular frequency, and v_{z_j} is velocity component in direction z of atom j. Fig. 3 illustrates the longitudinal phonon DOS for CNTs and GNTs at different MD temperatures. The DOS of armchair CNT is well defined in the literature and shows a strong peak at 48 THz (~1600 cm^{-1}) and a weaker peak at around 20 THz which are attributed to sp^2 bonding networks stretching and bending modes [41–43]. As can be seen, the total DOS of all GNTs demonstrate two peaks at around 48 THz and 64 THz, which can be attributed to the stretching of C—C (i.e. carbon-carbon bond with partial double bond character), and C≡C bonds respectively. There is also a peak at 33 THz for α and β-GNTs, which can be attributed to the interaction or combined stretching of two C—C and one C≡C bonds in series, $\nu_{combined} = \left(\frac{1}{\nu_{C-C}^2} + \frac{1}{\nu_{C\equiv C}^2} + \frac{1}{\nu_{C-C}^2}\right)^{-1/2}$, at the edge of graphyne hexagons.

By comparing the total DOS of GNTs and CNTs it was observed that as the percentage of carbon triple bonds in the structure increases, a larger number of high-energy phonon modes become available due to the dominance of the higher stretching frequency of carbon triple bonds. In addition, based on the Bose-Einstein distribution, as the temperature increases more high-energy modes become occupied, resulting in more scattering events and a broadening of characteristic peaks in DOS.

3.3. Phonon dispersion relation and relaxation time

The phonon dispersion relations are obtained for longitudinal, transverse, torsional, and radial modes as follows. In the first step, the normal mode amplitude, A(k, p, t), is calculated by converting the atomic trajectories obtained from MD to the reciprocal space as shown in Eq. (6).

$$A(k,p,t) = \sum_{j=1}^{N} (r_j(t) - r_{0j}) \cdot P_j(k,p) \cdot e^{-ik \cdot r_{0_j}} \tag{6}$$

where $r_j(t)$ is instantaneous position of atom j, $r_{0,j}$ its lattice position, and Pj the corresponding polarization vector. The phonon dispersion (k-ω) curves are obtained by transforming the normal mode autocorrelation function into the frequency domain and recording the dominant phonon frequency at each wave vector k. Fig. 3 illustrates the dispersion curves of armchair GNTs and CNTs along with the phonon density of states at a number of MD temperatures, and Fig. 4 shows similar data for zigzag CNTs and GNTs. As can be seen in Figs. 3 and 4, the phonon dispersion is found to be linear for all tubes, which contrasts with that for graphene sheets. Based on elasticity theory, non-linear (parabolic) flexural modes are known to exist in graphene and nanotubes [44]. Ref. [45] discusses emergence of parabolic flexural mode in relation to the rigid rotational invariance of potentials such as the Brenner type used in the numerical study. Although the transverse bands are seen here to exhibit a linear dependence with wave vector, for very small values of k (for very small frequencies), they do bend slightly. This could be consistent with parabolic behavior [46], but numerical errors cannot be fully ruled out. Compared with CNTs, GNTs demonstrate a considerably lower acoustic branch frequency at the edges of the Brillouin zone and lower slope $\frac{\delta\omega}{\delta k}$ at the gamma high symmetry point (i.e. lower phonon group velocity) at all polarizations. Table 2 lists values of phonon group velocities at different polarizations, which demonstrates that among GNTs, γ-GNT has the highest phonon group velocity at all polarizations for both zigzag and armchair nanotubes.

The frequency-dependent phonon relaxation times were calculated using the normal mode amplitude autocorrelation function. *ACF(A(k, p, t))* demonstrates an exponential decay with a time constant given by the phonon relaxation time τ [21]. It is

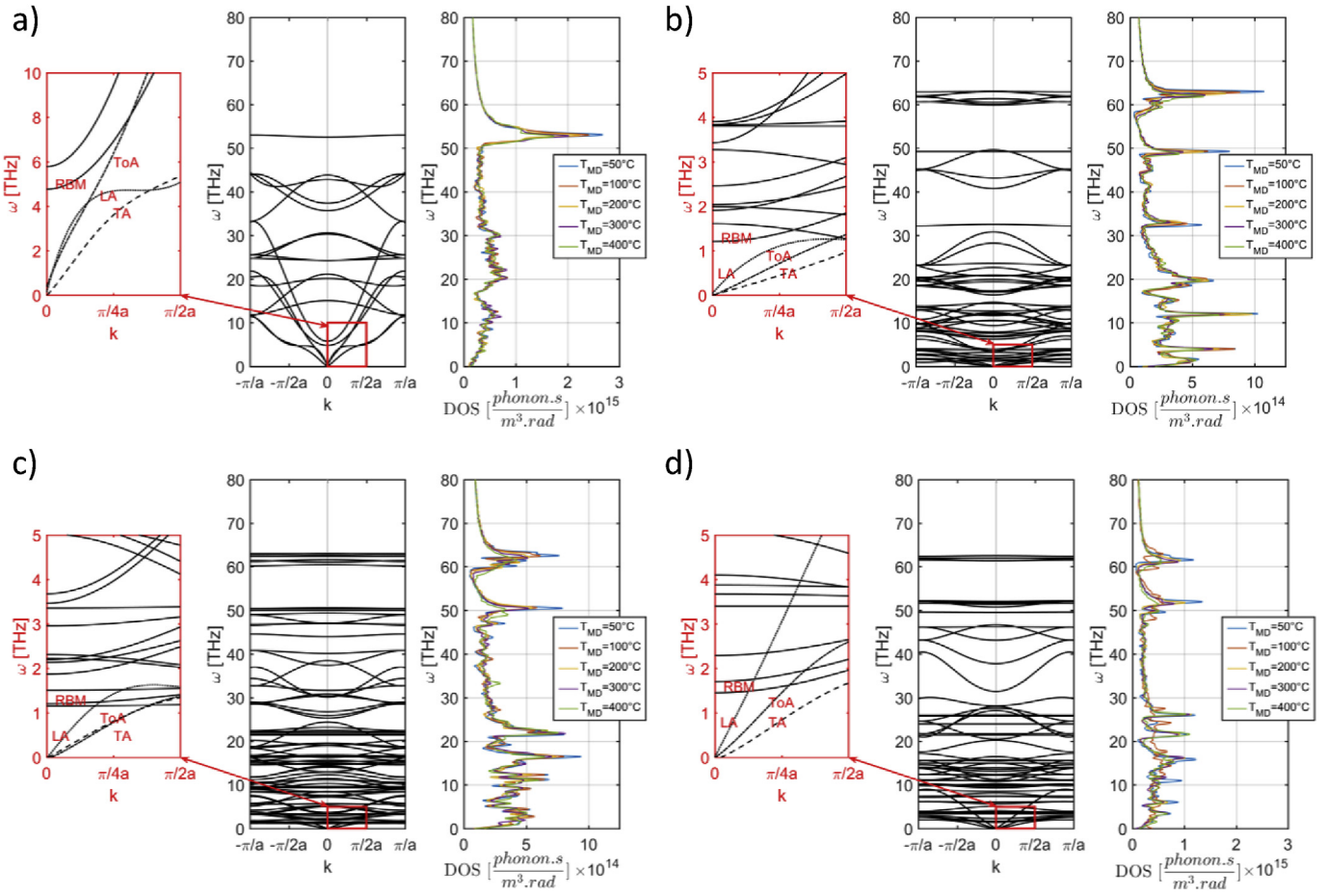

Fig. 3. Phonon dispersion relations and total phonon density of states at different temperatures for (a) (11, 11) armchair-CNT (b) armchair α-GNT (c) armchair β-GNT, and (d) armchair γ-GNT. (A colour version of this figure can be viewed online.)

noteworthy that the phonon relaxation times obtained from MD simulations include third and higher order phonon-phonon scattering, and do not distinguish between normal and Umklapp scattering and reflect a combined phonon-phonon scattering process. Fig. 5 illustrates LA phonon relaxation times as a function of frequency for all the modeled nanotubes. It can be seen that GNTs have considerably lower LA phonon relaxation times than CNTs. In addition, in all the cases considered the phonon relaxation time decreases with increasing frequency. This observation is consistent with previous studies, where a non-monotonic decrease of relaxation time with frequency was reported for other materials such as silicon and solid [21,47,48], indicating that higher frequency phonons are more dispersive. The dependence of relaxation time on frequency can be modeled with a power law form $\tau \propto \nu^{-n}$. The results show the following general trend in the order of dependence of LA phonon relaxation time on frequency for different nanotubes: $n_{\alpha\text{-}GNT} > n_{\beta\text{-}GNT} > n_{\gamma\text{-}GNT} > n_{CNT}$.

The phonon mean free path in polarization i can be obtained using the phonon group velocity and relaxation time based on the relation: $\lambda_i(k) = u_i(k) \cdot \tau_i(k)$. Fig. 6 depicts the acoustic phonon mean free path at different polarizations and temperatures for GNTs and CNTs. Compared with CNTs, GNTs demonstrate significantly lower MFPs at all polarizations. Among GNTs, by increasing the fraction of carbon triple bonds the MFP decreases and α-GNT, with the highest fraction of carbon triple bonds, has the lowest MFP. This can be attributed to more dispersive high frequency phonons which result in shorter relaxation times [21], as well as a lower phonon group velocity (as indicated in Table 2).

It can be seen that due to the significantly shorter MFP compared to the length of the nanotube, α and β-GNTs are operating in the diffusive transport regime at all the MD temperatures for the length of nanotube considered here (i.e. 50 nm). This is not the case for γ-GNT and CNTs, which have MFP values comparable to the nanotube length at mid to lower temperatures, which is an indication of ballistic or ballistic-diffusive transport. To determine the exact point of transition from ballistic to diffusive transport requires a change in the length of the simulated system. Nevertheless, in the case of CNTs, the presented results are in agreement with previous studies [49,50], which indicate ballistic transport in the mid to lower temperature range for the length of nanotubes considered here.

3.4. Quantum correction

Since quantum effects, which are neglected in classical MD calculation, are important at temperatures lower than Debye temperature, the MD calculations need to be quantum corrected at these temperatures [51,52]. We start by calculating the Debye temperature for each of the nanotubes, using the number of modes in an acoustic branch, which is equal to the number of primitive cells in the domain as shown in Eq. (7) [53].

$$M = \frac{N}{n} = V \int_0^{\upsilon_D} D_{tot}(\nu)\, d\nu \tag{7}$$

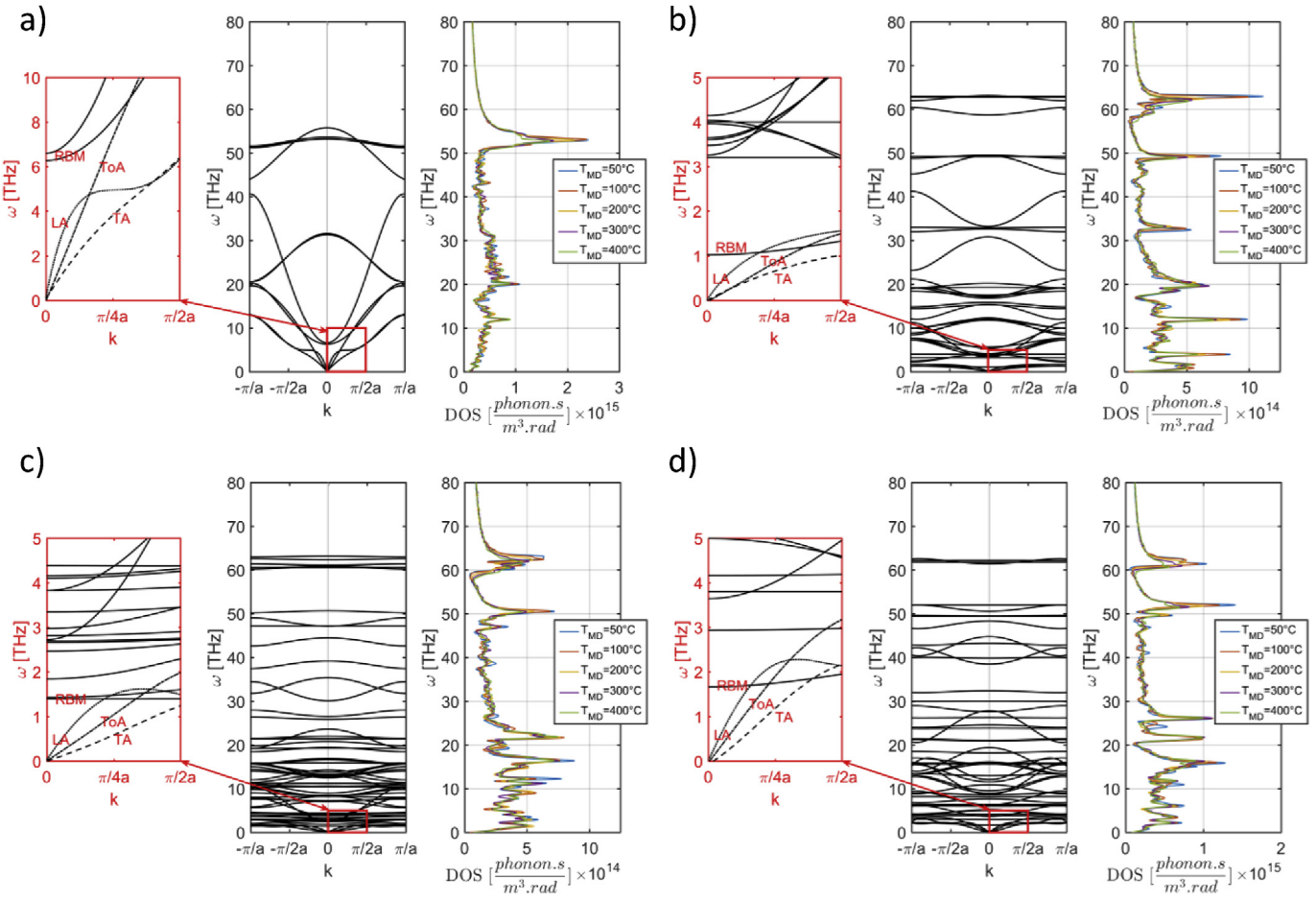

Fig. 4. Phonon dispersion relations and total phonon density of states at different temperatures for (a) (19, 0) zigzag-CNT (b) zigzag α-GNT (c) zigzag β-GNT, and (d) zigzag γ-GNT. (A colour version of this figure can be viewed online.)

Table 2
Phonon group velocities, Debye temperatures, and molar density of simulated nanotubes.

Nanotube type	C_{LA} (km s^{-1})	C_{TA} (km s^{-1})	C_{ToA} (km s^{-1})	T_D (K)	ρ (mol lit^{-1})
GNT α-arm	9.83	2.36	3.92	160.79	89.2
GNT α-zig	10.73	3.99	3.86	241.63	88.3
GNT β-arm	14.22	6.33	4.72	279.27	109.2
GNT β-zig	14.50	3.66	6.52	205.65	110.0
GNT γ-arm	16.09	3.21	6.06	226.06	141.7
GNT γ-zig	15.29	4.45	8.98	313.67	141.7
CNT arm	26.23	7.17	12.68	468.55	191.7
CNT zig	26.23	8.03	11.34	509.85	192.5

The total density of states based on the Debye model, $D_{Deb,tot}$, for four acoustic branches, including 1 longitudinal acoustic (LA), 2 degenerate transverse acoustic (TA), and 1 torsional acoustic (ToA) [22], can be obtained from Eq. (8) by assuming linear dispersion curves (i.e. $\omega = C_{av}k$).

$$D_{Deb\cdot tot}(\upsilon) = \frac{2\upsilon^2}{u_{av}^3}$$
$$4\frac{1}{u_{av}^3} = \frac{1}{u_{LA}^3} + \frac{2}{u_{TA}^3} + \frac{1}{u_{ToA}^3} \quad (8)$$

The Debye temperature, T_D, can be evaluated by evaluating the integral of Eq. (7) using the density of states obtained in Eq. (8), as shown in Eq. (9).

$$\upsilon_D = \left(\frac{3\,u_{av}^3 M}{4\pi V}\right)^{1/3} = \frac{k_B T_D}{h} \quad (9)$$

The LA, TA, and ToA group velocities, as well as the Debye temperatures for each nanotube are listed in Table 2. For all cases,

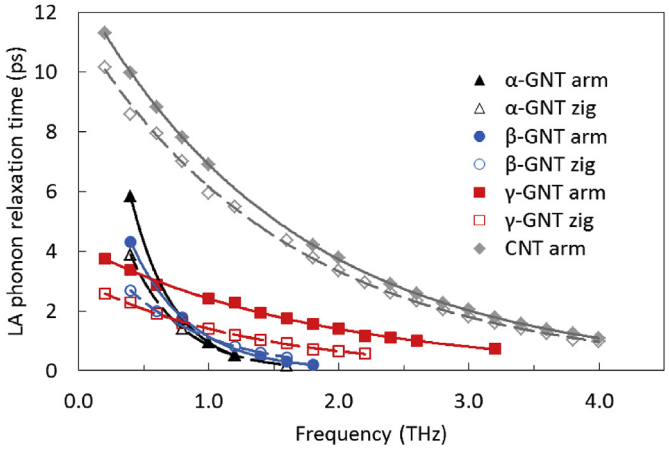

Fig. 5. LA phonon relaxation time as a function of frequency. (A colour version of this figure can be viewed online.)

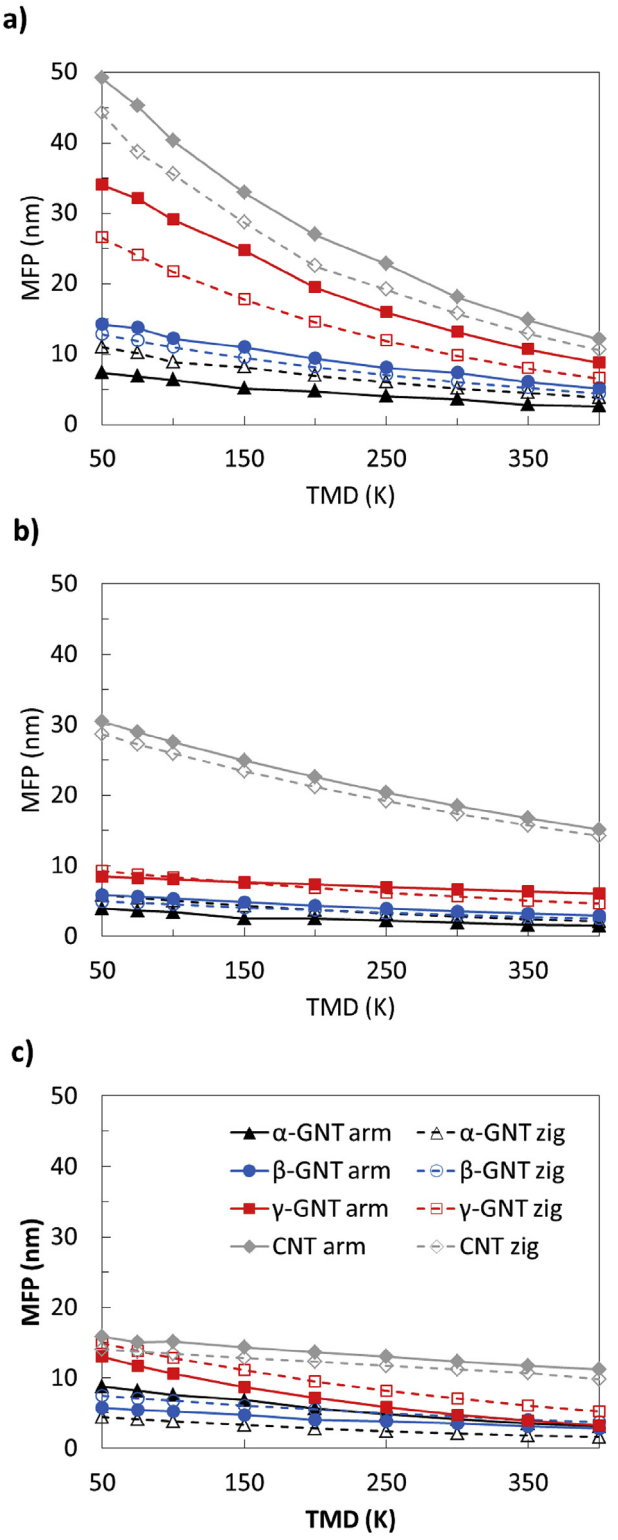

Fig. 6. Mean free path at different MD temperatures for (a) LA, (b) TA, and (c) ToA modes. (A colour version of this figure can be viewed online.)

the Debye temperature is within or higher than the MD temperature range, which necessitates the quantum correction. The Debye temperature values for CNTs are comparable with the values reported of 473 [22], 475 [54], and 580 [55]. Also, it can be seen that the Debye temperature of GNTs are significantly less than CNTs, which is due to lower atomic network density and average group velocity. Therefore, compared to CNTs, which need consideration of quantum effects even at room temperature [12], GNTs are less prone to quantum effects at room temperature.

The quantum temperature, T, is calculated by equating the total system energy at T_{MD} to the total phonon energy at T using the Debye model for density of states as shown in Eq. (10) [52]. The relation between T_{MD} and T obtained from this equation is shown in supplementary information (Fig. S1), which indicates deviation of T_{MD} from T at low temperatures and approaching the T value at high temperatures.

$$E = 3\,k_B\,T_{MD}\int_0^{\upsilon_D} d\upsilon\; h\nu\; D_{Deb\cdot tot}(\upsilon)\left(\frac{1}{e^{\frac{h\nu}{k_B T}}-1}+\frac{1}{2}\right) \tag{10}$$

Using the chain rule, the thermal conductivity obtained from MD calculations can be quantum corrected by multiplying to dT_{MD}/dT [56]. Fig. 2 (b) illustrates the corrected values of the longitudinal thermal conductivity.

3.5. Phonon specific heat

The specific heat in carbon nanotubes is dominated by the phonon contribution C_{ph}. C_{ph} can be calculated by taking the derivative of total energy using the total density of states $D_{MD.\,tot}$ integrated over a wide range of frequencies as shown in Eq. (11) [20,52].

$$\begin{aligned} C_{ph} &= \left[\frac{\partial E}{\partial T}\right]_V = \frac{\partial}{\partial T}\left(\int_0^{\upsilon_{max}} D_{MD\cdot tot}(\upsilon)\frac{h\nu\, d\nu}{e^{\frac{h\nu}{k_B T}}-1}\right) \\ &= \int_0^{\upsilon_{max}} k_B\left(\frac{h\upsilon}{k_B T}\right)^2 D_{MD\cdot tot}(\upsilon)\frac{e^{\frac{h\nu}{k_B T}}h\nu\, d\nu}{\left(e^{\frac{h\nu}{k_B T}}-1\right)^2} \end{aligned} \tag{11}$$

Molar heat capacities for all the nanotubes fall in a narrow range as shown in Fig. 7 (a), with α, β, and γ-GNTs having the highest values respectively and CNTs having noticeably lower values. As observed in Figs. 3 and 4, nanotubes with a larger percentage of C≡C bonds have a larger number of high-energy modes, which contribute to larger values of the heat capacity.

Based on Eq. (4), the thermal conductivity is proportional to the volumetric heat capacity, which is shown in Fig. 7 (b). CNTs have considerably higher volumetric heat capacity than do GNTs; among GNTs, γ, β, and α-GNTs have successively smaller molar heat capacities. Since the molar heat capacity values are within a narrow range, the volumetric heat capacity is mainly a function of atomic network density of nanotubes. Therefore, atomic network density is one of the main contributing factors to the difference in thermal conductivity of different GNTs and CNTs. The molar densities (ρ), calculated based on a ring with a van der Waals thickness of 3.4 Å [57], are listed in Table 2, which shows considerably higher values for CNTs than for GNTs.

4. Potential applications for energy conversion: phonovoltaics

The phonon transport properties of GNTs, their high-energy optical phonons and relatively low thermal conductivities, suggest potential uses of GNTs in energy conversion applications. Here we focus on potential applications of GNTs in phonovoltaic devices. First suggested by C. Melnick and M. Kaviani [9], phonovoltaic devices harvest nonequilibrium optical phonons ($E_{p,O}$) more energetic than the band gap (ΔE_g) to generate electron-hole pairs, which are then separated in a p-n junction. A potential phonovoltaic material

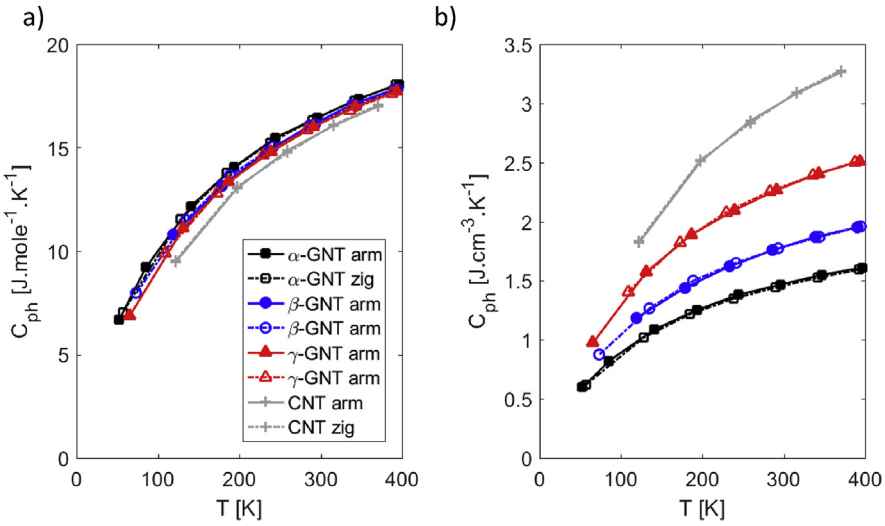

Fig. 7. (a) Molar and (b) volumetric phonon heat capacity of GNTs and CNTs. (A colour version of this figure can be viewed online.)

satisfies $E_{p,O} \approx \Delta E_{\Delta g} \gg k_B T$, and has a strong interband electron-phonon coupling. In addition, graphyne sheets and GNTs have already been shown to have a high thermoelectric figure of merit, due to lower thermal conductivity and considerably higher Seebeck coefficient than graphene, making the former the preferred materials for thermoelectric power generation [58–61].

The electronic band structure, obtained from first-principle density-functional calculations in Ref. [62], indicates that $\Delta E_g = 0$ for α- and β-graphyne sheets. For γ-GNT, the band gap of 0.471 eV is higher than the maximum optical phonon energy (~0.26 eV), which is undesirable for phonovoltaic applications. However, it has been shown that rolling a sheet of α-graphyne into a α-GNT opens up a band gap that can be tuned by varying the diameter of the nanotube [63]. As can be seen in Fig. 8 (a), the band gap of armchair α-GNT is too low compared to $E_{p,O}$ ~0.26 eV, whereas the band gap of zigzag α-GNT can be precisely tuned to the range of optical phonon energy of zigzag α-GNT by varying the GNT diameter. In Fig. 8 (b) the band structure of three zigzag α-GNT candidates with diameters of 1.56 nm, 2.22 nm, and 2.89 nm (corresponding to indices of (7, 0), (10, 0), and (13, 0) respectively) are shown along with the high-energy optical phonon dispersion curves, and total phonon density of states. It can be seen that for two cases of D = 2.22 nm and 2.89 nm the requirements $E_{p,O} \approx \Delta E_{\Delta g} \gg k_B T$ for a phonoelectric material are completely met, and the optical phonons, at ~0.26 eV generated by carbon triple bonds, can excite the direct band gap and is one order of magnitude higher than the thermal energy at 300 K. In the case of D = 2.89 mm, the highly populated optical phonons at ~0.20 eV can also excite the bandgap, indicating that a considerable portion of optical phonons can be potentially be harvested in a phonovoltaic device. Based on the electron and phonon band structures and high population number of high-energy optical phonons, the zigzag α-GNT is suggested as a potential candidate for phonovoltaic applications. However, further analysis is required to determine the role of electron phonon-coupling in such GNT structures where the phonovoltaic energy conversion is energetically favorable.

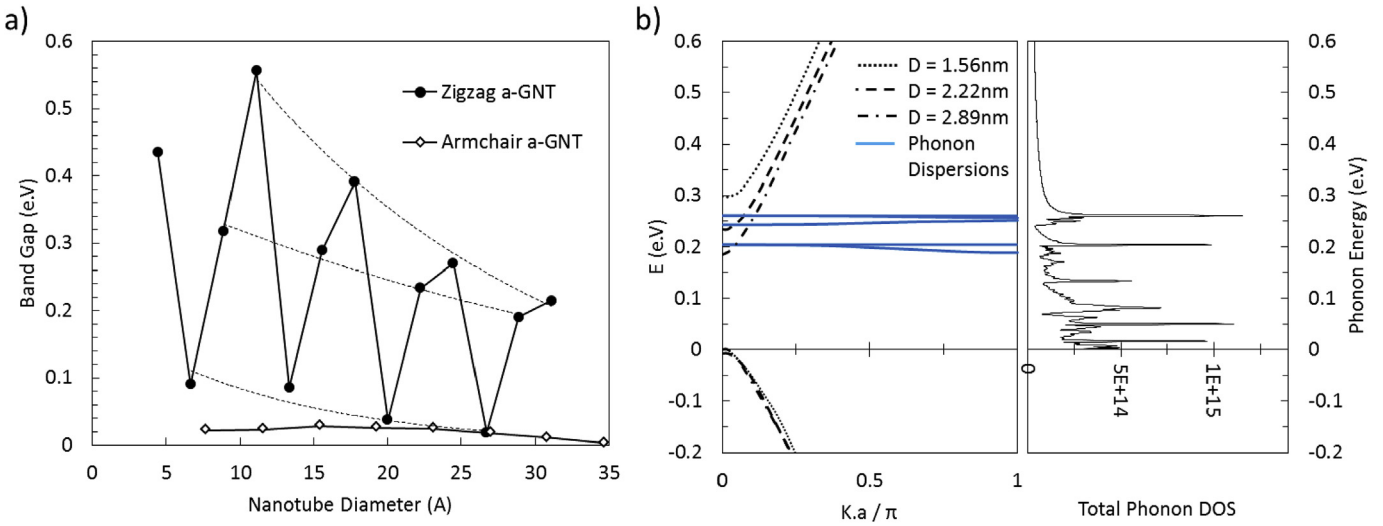

Fig. 8. (a) Band gap of zigzag and armchair α-GNTs as a function of nanotube diameter, from Ref. [63] and (b) The dashed lines show the band structure of three zigzag α-GNTs with diameters of 1.56 nm, 2.22 nm, and 2.89 nm, from Ref. [63]. The high-energy optical phonon dispersion curves of zigzag α-GNTs with diameter of 2.22 nm are shown with blue lines, and the corresponding phonon density of states are shown on the right plot. (A colour version of this figure can be viewed online.)

5. Conclusion

Using molecular dynamics simulations, along with quantum corrections, the role of carbon triple bonds in thermal transport properties of carbon and graphyne nanotubes has been determined. Based on the phonon density of states in Figs. 3 and 4, more high-energy optical phonons modes become available with increasing percentage of carbon triple bonds. As indicated by Fig. 5, addition of these high-energy optical phonons increases the phonon-phonon scattering and leads to shorter acoustic phonon relaxation times. In addition, the LA and ToA phonon group velocities demonstrate a monotonic decrease, and the TA mode shows a non-monotonic decrease with increasing percentage of carbon triple bonds. This, in conjunction with shorter phonon relaxation time, leads to a shorter mean free path (as indicated in Fig. 6) for nanotubes such as α-GNTs with more triple bonds. Moreover, the molar phonon heat capacity slightly increases due to higher occupation number of high-energy phonons. On the other hand, the volumetric phonon heat capacity significantly decreases with increasing numbers of triple bonds due to a decrease in the atomic network density, which contributes to the decrease in thermal conductivity.

We concluded that the thermal conductivity of GNTs are considerably lower than CNTs, and among GNTs, α and β-GNT demonstrates noticeably lower thermal conductivities compared to γ-GNT due to the following reasons: (1) A Significantly lower acoustic group velocity (2) shorter phonon relaxation times and acoustic phonon mean free path, and (3) lower volumetric phonon heat capacity. In addition, α-GNT demonstrates the highest population of high-energy (0.26 eV) optical phonons, which are significantly more energetic than the thermal energy at room temperature. The band gap of zigzag α-GNT can be tuned to harvest the energy of these optical phonons. Based on the electronic and phonon band structure, the (10, 0) and (13, 0) α-GNTs are suggested as potential phonovoltaic energy conversion materials. Future study is encouraged to determine the role of electron phonon-coupling in such GNT structures where the phonovoltaic energy conversion is energetically favorable.

Conflict of interest

The authors declare no competing financial interest.

Acknowledgement

The authors would like to acknowledge the use of University of Michigan's Advanced Research Computing Cluster for carrying out the simulations.

Nomenclature

$C-C$	Carbon-carbon bond with partial double bound character
$C\equiv C$	Carbon-carbon triple bond
LA	Longitudinal acoustic
LO	Longitudinal optic
TA	Transverse acoustic
TO	Transverse optic
ToA	Torsional acoustic
ToO	Torsional optic
RBM	Radial breathing mode
L	Nanotube length
D	Nanotube diameter
t	Time
$K_{i,j}$	Thermal conductivity tensor
V	System volume
k_B	Boltzmann constant
T_{MD}	Molecular dynamics temperature
J	Heat flux vector
e_i	Total energy of atom i
S_i	Stress tensor of atom i
v_i	Velocity vector of atom i
v_{ji}	Velocity in direction j of atom i
C_{ph}	Phonon heat capacity
u_i	Phonon group velocity in direction i
ACF	Autocorrelation function
τ	Phonon relaxation time
λ	Phonon mean free path
D_i	Density of state for phonon mode i
N	Total number of atoms
M	Number of primitive cells in the computational domain
n	Number of atoms in primitive cell
ω	Phonon angular frequency
ν	Phonon frequency
A	Normal mode amplitude
k	Wave vector
p	Polarization
r_i	Position of atom i
$r_{0\ i}$	Lattice position of atom i
P_i	Polarization vector of atom i
υ_D	Debye frequency
T_D	Debye temperature
u_{av}	Average phonon group velocity
h	Planck constant
$D_{Deb.tot}$	Density of states based on Debye model
E	Total energy
D_i	Density of state in polarization i
$E_{p,O}$	Optical phonon energy
ΔE_g	Band gap

Appendix A. Supplementary data

Supplementary data related to this article can be found at http://dx.doi.org/10.1016/j.carbon.2017.07.093.

References

[1] Andrey K Geim, Allan H. MacDonald, Graphene: exploring carbon flatland, Phys. Today 60 (8) (2007).
[2] M.-H. Shih, L.-J. Li, Y.-C. Yang, H.-Y. Chou, C.-T. Lin, C.-Y. Su, Efficient heat dissipation of photonic crystal microcavity by monolayer graphene, ACS Nano 7 (12) (2013) 10818–10824.
[3] C. Subramaniam, Y. Yasuda, S. Takeya, S. Ata, A. Nishizawa, D. Futaba, T. Yamada, K. Hata, Carbon nanotube-copper exhibiting metal-like thermal conductivity and silicon-like thermal expansion for efficient cooling of electronics, Nanoscale 6 (5) (2014) 2669–2674.
[4] Q. Yao, L. Chen, W. Zhang, S. Liufu, X. Chen, Enhanced thermoelectric performance of single-walled carbon nanotubes/polyaniline hybrid nanocomposites, Acs Nano 4 (4) (2010) 2445–2451.
[5] C. Yu, Y. Ryu, L. Yin, H. Yang, Modulating electronic transport properties of carbon nanotubes to improve the thermoelectric power factor via nanoparticle decoration, ACS Nano 5 (2) (2011) 1297–1303.
[6] A. Lenert, D.M. Bierman, Y. Nam, W.R. Chan, I. Celanović, M. Soljačić, E.N. Wang, A nanophotonic solar thermophotovoltaic device, Nat. Nanotechnol. 9 (2) (2014) 126–130.
[7] R. St-Gelais, G.R. Bhatt, L. Zhu, S. Fan, M. Lipson, Hot carrier-based near-field thermophotovoltaic energy conversion, ACS Nano 11 (3) (2017) 3001–3009.
[8] M. Maldovan, Phonon wave interference and thermal bandgap materials, Nat. Mater. 14 (7) (2015) 667–674.
[9] C. Melnick, M. Kaviany, Phonovoltaic. I. Harvesting hot optical phonons in a nanoscale p–n junction, Phys. Rev. B 93 (9) (2016) 094302.
[10] C.A. Hewitt, A.B. Kaiser, S. Roth, M. Craps, R. Czerw, D.L. Carroll, Multilayered carbon nanotube/polymer composite based thermoelectric fabrics, Nano Lett. 12 (3) (2012) 1307–1310.
[11] K. Yanagi, S. Kanda, Y. Oshima, Y. Kitamura, H. Kawai, T. Yamamoto, T. Takenobu, Y. Nakai, Y. Maniwa, Tuning of the thermoelectric properties of one-dimensional material networks by electric double layer techniques using ionic liquids, Nano Lett. 14 (11) (2014) 6437–6442.

[12] A.M. Marconnet, M.A. Panzer, K.E. Goodson, Thermal conduction phenomena in carbon nanotubes and related nanostructured materials, Rev. Mod. Phys. 85 (3) (2013) 1295.
[13] E. Pop, D. Mann, Q. Wang, K. Goodson, H. Dai, Thermal conductance of an individual single-wall carbon nanotube above room temperature, Nano Lett. 6 (1) (2006) 96–100.
[14] M. Fujii, X. Zhang, H. Xie, H. Ago, K. Takahashi, T. Ikuta, H. Abe, T. Shimizu, Measuring the thermal conductivity of a single carbon nanotube, Phys. Rev. Lett. 95 (6) (2005) 065502.
[15] P. Kim, L. Shi, A. Majumdar, P. McEuen, Thermal transport measurements of individual multiwalled nanotubes, Phys. Rev. Lett. 87 (21) (2001) 215502.
[16] Q. Li, C. Liu, X. Wang, S. Fan, Measuring the thermal conductivity of individual carbon nanotubes by the Raman shift method, Nanotechnology 20 (14) (2009) 145702.
[17] W. Yi, L. Lu, Z. Dian-Lin, Z. Pan, S. Xie, Linear specific heat of carbon nanotubes, Phys. Rev. B 59 (14) (1999). R9015.
[18] S. Berber, Y.-K. Kwon, D. Tománek, Unusually high thermal conductivity of carbon nanotubes, Phys. Rev. Lett. 84 (20) (2000) 4613.
[19] M. Dresselhaus, P. Eklund, Phonons in carbon nanotubes, Adv. Phys. 49 (6) (2000) 705–814.
[20] J. Hone, Phonons and Thermal Properties of Carbon Nanotubes, Carbon Nanotubes, Springer, 2001, pp. 273–286.
[21] A.S. Henry, G. Chen, Spectral phonon transport properties of silicon based on molecular dynamics simulations and lattice dynamics, J. Comput. Theor. Nanosci. 5 (2) (2008) 141–152.
[22] J.R. Lukes, H. Zhong, Thermal conductivity of individual single-wall carbon nanotubes, J. Heat Transf. 129 (6) (2007) 705–716.
[23] Y. Huang, Q. Gong, Q. Zhang, Y. Shao, J. Wang, Y. Jiang, M. Zhao, D. Zhuang, J. Liang, Fabrication and molecular dynamics analyses of highly thermal conductive reduced graphene oxide films at ultra-high temperatures, Nanoscale 9 (6) (2017) 2340–2347.
[24] G. Balasubramanian, I.K. Puri, M.C. Böhm, F. Leroy, Thermal conductivity reduction through isotope substitution in nanomaterials: predictions from an analytical classical model and nonequilibrium molecular dynamics simulations, Nanoscale 3 (9) (2011) 3714–3720.
[25] R.N. Salaway, L.V. Zhigilei, Molecular dynamics simulations of thermal conductivity of carbon nanotubes: resolving the effects of computational parameters, Int. J. Heat Mass Transf. 70 (2014) 954–964.
[26] J. Hu, X. Ruan, Y.P. Chen, Thermal conductivity and thermal rectification in graphene nanoribbons: a molecular dynamics study, Nano Lett. 9 (7) (2009) 2730–2735.
[27] J. Wang, A.-J. Zhang, Y. Tang, Tunable thermal conductivity in carbon allotrope sheets: role of acetylenic linkages, J. Appl. Phys. 118 (19) (2015) 195102.
[28] Y. Zhang, Q. Pei, C. Wang, A molecular dynamics investigation on thermal conductivity of graphynes, Comput. Mater. Sci. 65 (2012) 406–410.
[29] M. Alaghemandi, E. Algaer, M.C. Böhm, F. Müller-Plathe, The thermal conductivity and thermal rectification of carbon nanotubes studied using reverse non-equilibrium molecular dynamics simulations, Nanotechnology 20 (11) (2009) 115704.
[30] D.J. Evans, Homogeneous NEMD algorithm for thermal conductivity—application of non-canonical linear response theory, Phys. Lett. A 91 (9) (1982) 457–460.
[31] W. Zhang, Z. Zhu, F. Wang, T. Wang, L. Sun, Z. Wang, Chirality dependence of the thermal conductivity of carbon nanotubes, Nanotechnology 15 (8) (2004) 936.
[32] A.A. Balandin, Thermal properties of graphene and nanostructured carbon materials, Nat. Mater. 10 (8) (2011) 569–581.
[33] R. Baughman, H. Eckhardt, M. Kertesz, Structure-property predictions for new planar forms of carbon: layered phases containing sp 2 and sp atoms, J. Chem. Phys. 87 (11) (1987) 6687–6699.
[34] C.-N. Pan, X.-K. Chen, L.-M. Tang, K.-Q. Chen, Orientation dependent thermal conductivity in graphyne nanoribbons, Phys. E Low Dimens. Syst. Nanostructures 64 (2014) 129–133.
[35] M. Hu, Y. Jing, X. Zhang, Low thermal conductivity of graphyne nanotubes from molecular dynamics study, Phys. Rev. B 91 (15) (2015) 155408.
[36] S.G. Volz, G. Chen, Molecular dynamics simulation of thermal conductivity of silicon nanowires, Appl. Phys. Lett. 75 (14) (1999) 2056–2058.
[37] W.J. Evans, L. Hu, P. Keblinski, Thermal conductivity of graphene ribbons from equilibrium molecular dynamics: effect of ribbon width, edge roughness, and hydrogen termination, Appl. Phys. Lett. 96 (20) (2010) 203112.
[38] A.P. Thompson, S.J. Plimpton, W. Mattson, General formulation of pressure and stress tensor for arbitrary many-body interaction potentials under periodic boundary conditions, J. Chem. Phys. 131 (15) (2009) 154107.
[39] A. Kumar, V. Sundararaghavan, A. Browning, Study of temperature dependence of thermal conductivity in cross-linked epoxies using molecular dynamics simulations with long range interactions, Model. Simul. Mater. Sci. Eng. 22 (2) (2014) 025013.
[40] S. Plimpton, Fast parallel algorithms for short-range molecular dynamics, J. Comput. Phys. 117 (1) (1995) 1–19.
[41] M.S. Dresselhaus, A. Jorio, M. Hofmann, G. Dresselhaus, R. Saito, Perspectives on carbon nanotubes and graphene Raman spectroscopy, Nano Lett. 10 (3) (2010) 751–758.
[42] U.J. Kim, C.A. Furtado, X. Liu, G. Chen, P.C. Eklund, Raman and IR spectroscopy of chemically processed single-walled carbon nanotubes, J. Am. Chem. Soc. 127 (44) (2005) 15437–15445.
[43] J. Mohan, Organic Spectroscopy: Principles and Applications, Crc Press, 2004.
[44] L.D. Landau, L.P. Pitaevskii, A.M. Kosevich, E.M. Lifshitz, Theory of Elasticity, third ed., Elsevier Ltd., 2012.
[45] J.W. Jiang, B.S. Wang, J.S. Wang, H.S. Park, A review on the flexural mode of graphene: lattice dynamics, thermal conduction, thermal expansion, elasticity and nanomechanical resonance, J. Phys. Condens. Matt. 27 (8) (2015).
[46] D. Sanchez-Portal, E. Hernandez, Vibrational properties of single-wall nanotubes and monolayers of hexagonal BN, Phys. Rev. B 66 (23) (2002).
[47] A.J. McGaughey, M. Kaviany, Quantitative validation of the Boltzmann transport equation phonon thermal conductivity model under the single-mode relaxation time approximation, Phys. Rev. B 69 (9) (2004) 094303.
[48] A.J. Ladd, B. Moran, W.G. Hoover, Lattice thermal conductivity: a comparison of molecular dynamics and anharmonic lattice dynamics, Phys. Rev. B 34 (8) (1986) 5058.
[49] N. Mingo, D. Broido, Length dependence of carbon nanotube thermal conductivity and the “problem of long waves”, Nano Lett. 5 (7) (2005) 1221–1225.
[50] J. Wang, J.-S. Wang, Carbon nanotube thermal transport: ballistic to diffusive, Appl. Phys. Lett. 88 (11) (2006) 111909.
[51] S. Sinha, K.E. Goodson, Review: multiscale thermal modeling in nanoelectronics, Int. J. Multiscale Comput. Eng. 3 (1) (2005).
[52] M.C. Wu, J.-Y. Hsu, Thermal conductivity of carbon nanotubes with quantum correction via heat capacity, Nanotechnology 20 (14) (2009) 145401.
[53] C. Kittel, Introduction to Solid State Physics, eighth ed., Wiley, New York, 2004.
[54] A. Charlier, E. McRae, M.-F. Charlier, A. Spire, S. Forster, Lattice dynamics study of zigzag and armchair carbon nanotubes, Phys. Rev. B 57 (11) (1998) 6689.
[55] J. Benoit, B. Corraze, O. Chauvet, Localization, Coulomb interactions, and electrical heating in single-wall carbon nanotubes/polymer composites, Phys. Rev. B 65 (24) (2002) 241405.
[56] Y.H. Lee, R. Biswas, C.M. Soukoulis, C. Wang, C. Chan, K. Ho, Molecular-dynamics simulation of thermal conductivity in amorphous silicon, Phys. Rev. B 43 (8) (1991) 6573.
[57] S. Maruyama, A molecular dynamics simulation of heat conduction of a finite length single-walled carbon nanotube, Microscale Thermophys. Eng. 7 (1) (2003) 41–50.
[58] X.-M. Wang, D.-C. Mo, S.-S. Lu, On the thermoelectric transport properties of graphyne by the first-principles method, J. Chem. Phys. 138 (20) (2013) 204704.
[59] H. Sevinçli, C. Sevik, Electronic, phononic, and thermoelectric properties of graphyne sheets, Appl. Phys. Lett. 105 (22) (2014) 223108.
[60] X.-M. Wang, S.-S. Lu, Thermoelectric transport in graphyne nanotubes, J. Phys. Chem. C 117 (38) (2013) 19740–19745.
[61] X. Tan, H. Shao, T. Hu, G. Liu, J. Jiang, H. Jiang, High thermoelectric performance in two-dimensional graphyne sheets predicted by first-principles calculations, Phys. Chem. Chem. Phys. 17 (35) (2015) 22872–22881.
[62] B.G. Kim, H.J. Choi, Graphyne: hexagonal network of carbon with versatile Dirac cones, Phys. Rev. B 86 (11) (2012) 115435.
[63] B. Kang, J.Y. Lee, Electronic properties of α-graphyne nanotubes, Carbon 84 (2015) 246–253.